nuclear fusion
IAEA

PAPER • OPEN ACCESS

Multi-pellet injection into the NBI-heated phase of TJ-II plasmas

To cite this article: K.J. McCarthy *et al* 2024 *Nucl. Fusion* **64** 066019

OPEN ACCESS
IOP Publishing | International Atomic Energy Agency
Nuclear Fusion
Nucl. Fusion **64** (2024) 066019 (15pp)
https://doi.org/10.1088/1741-4326/ad4047

Multi-pellet injection into the NBI-heated phase of TJ-II plasmas

K.J. McCarthy[1,*], I. García-Cortés[1], J.A. Alonso[1], A. Arias-Camisón[2], E. Ascasíbar[1], A. Baciero[1], A. Cappa[1], R. Carrasco[1], O.O. Chmyga[3], T. Estrada[1], R. García[1], J. Hernández-Sánchez[1], F.J. Hernanz[1], O.S. Kozachok[3], B. López Miranda[1], F. Medina[1], D. Medina-Roque[1], B. van Milligen[1], M. Navarro[1], M.A. Ochando[1], J.L. de Pablos[1], N. Panadero[1], I. Pastor[1], J. de la Riva[1], M. C. Rodríguez[1], D. Tafalla[1], V. Tribaldos[4] and TJ-II Team[a]

[1] Laboratorio Nacional de Fusión, CIEMAT, Madrid, Spain
[2] Facultad de Ciencias Físicas, Universidad de Salamanca, Salamanca, Spain
[3] Kharkov Institute of Physics and Technology, Kharkiv, Ukraine
[4] Universidad Carlos III de Madrid, Leganés, Madrid, Spain

E-mail: kieran.mccarthy@ciemat.es

Received 12 January 2024, revised 1 April 2024
Accepted for publication 18 April 2024
Published 1 May 2024

Abstract

A pellet-induced enhanced confinement (PiEC) phase, with general characteristics similar to those reported for the stellarator W7-X, is observed after single pellet injection ($>10^{19}$ H atoms) into the neutral beam injection heated phase of plasmas in the mid-sized heliac-type stellarator TJ-II. In addition to a step-like increase in density, plasma diamagnetic energy content rises significantly with respect to that of reference discharges, energy confinement time is similarly enhanced when compared to International Stellarator Scaling law predictions (Yamada *et al* 2005 *Nucl. Fusion* **45** 1684) renormalized for TJ-II, and the triple product, $n_e \cdot T_i \cdot \tau_E$, exhibits a clear bifurcation towards an improved confinement branch when compared to the branch product predicted by the same law. In this work, multiple pellets are injected in series into NBI-heated plasmas in the TJ-II and post-injection plasma performance is reported and discussed. For instance, a charge-exchange recombination spectroscopy diagnostic reveals significantly increased core ion temperatures after pellet injection compared to temperatures achieved in comparable reference plasmas, this pointing to increased ion energy content and improved ion energy confinement during a PiEC phase. It is also found that enhanced performance is independent of whether co- or counter-NBI heating beam is employed. Finally, record stored diamagnetic energy content and plasma beta values are achieved when the largest available pellets are employed. The results indicate that pellet injections extend the operational regime well beyond limits previously achieved in TJ-II without pellets.

[a] See C. Hidalgo *et al* 2022 (https://doi.org/10.1088/1741-4326/ac2ca1) for the TJ-II Team.
[*] Author to whom any correspondence should be addressed.

Keywords: stellarator, pellet, confinement, operational regime

(Some figures may appear in colour only in the online journal)

1. Introduction

Cryogenic pellet injection (PI) is widely employed on magnetic confinement fusion (MCF) devices to fuel the plasma core [1]. Indeed, pellet technology is now well developed and injectors are employed on most MCF machines [2]. In the case of tokamaks, it has been demonstrated that fuelling is best achieved when injecting pellets from the high-field side (HFS) whereas, in the case of stellarators, it is still to be determined if HFS or low-field side (LFS) injections are more advantageous [3]. In addition, improved plasma performance, associated with pellet fuelling, has been reported for both device types [4–7]. Indeed, improved performance rather than fuelling is the principal interest of the work presented here. For instance, a common post-injection characteristic is a clear increase in plasma energy confinement compared to that achieved for gas puff and/or recycling fuelled discharges. This work is motivated by the previous identification of an enhanced performance phase after the injection of a single pellet into neutral beam injector (NBI) heated plasmas of the medium-sized stellarator TJ-II [8, 9]. The focus here is on multi-pellet injections and is aimed at further investigating and extending such an enhanced operational regime. Multi-pellet injection studies have been performed in other stellarator devices such as the Large Helical Device (LHD) [10] and Wendelstein 7-X (W7-X) [11]. In the case of W7-X, a short-lived high-performance phase was achieved after multi-pellet injections into microwave heated discharges when additional post-injection heating power was applied. It was reported then that the plasma moves to a different enhanced branch of the triple product, $n_e \cdot T_i \cdot \tau_E$, after these PIs [12]. However, this branch was transient and diminished as plasma density decayed. A more negative radial electric field was also observed during this post-pellet enhanced confinement phase [13], it being mainly reproduced by neoclassical simulations. In the case of LHD, multi-pellet injection was used to create an internal diffusion barrier (IDB) that resulted in an increase in core density and large radial density gradients. Once developed, the IDB structure was maintained well after injections were completed, thereby extending its improved confinement regime ([14] and references therein).

In TJ-II, pellet studies have focussed on pellet ablation and deposition physics [15, 16] as well as on fuelling efficiency [17]. However, more recently, it was reported that the injection of a single cryogenic pellet into the NBI-heated phase of a discharge enhanced plasma performance that was sustained until beam switch-off [9]. Therein, it was reported that energy confinement increased significantly compared to predictions from the ISS04 Scaling law for TJ-II [18, 19]. It was reported also that the pellet-induced enhanced performance (PiEC) phase was characterized by more negative radial density gradients around $\rho = 0.6$, by more negative plasma potentials in the plasma core, and by reductions in density fluctuations in the region of steepest density gradients. Here $\rho = r/a$, r is plasma radius and a is normalized plasma minor radius. Moreover, in the same paper, a clear bifurcation point towards an improved confinement branch was observed when the experimental triple product, $n_e \cdot T \cdot \tau_E{}^{diag}$, was compared to the product branch predicted by the International Stellarator Scaling law for TJ-II. Experimental observations also indicated increased peaking of core radiation losses which pointed to edge/core plasma decoupling. It was noted also that while not enabling identification of a mechanism for improved performance, NeoClassical (NC) calculations predicted more negative radial electric field, E_r, and increased energy confinement times, which agreed qualitatively, although not quantitatively, with experimental tendencies. This indicated that turbulence might be playing a significant role in this phenomenon. More recently, a dynamical turbulence mechanism that may explain TJ-II observations, to some extent at least, was studied using a model based on resistive magnetohydrodynamic (MHD) equations [20]. It was considered that the more negative density gradients induced by a pellet may excite resistive interchange modes close to low-order rational surfaces. In turn, it was deemed also that such instabilities show strong mutual coupling and create multiple transport barriers through associated zonal flows. Then, in such cases, via Reynolds stress, these may generate a strongly negative electrostatic potential (associated with E_r and with sheared flow). Finally, it was postulated that such a strongly non-linear dynamic process may play an important role in the observed post-pellet confinement improvements in TJ-II. Studies to obtain further insight into this topic are being undertaken currently and will be published at a later date.

In this work, series of cryogenic hydrogen pellets are injected into the NBI-heated phase of TJ-II discharges with the aim of identifying and quantifying performance improvements and plasma evolution after multiple injections when compared to improvements after a single pellet injection. For instance, series of the largest pellets available are injected in order to investigate operational limits for this PiEC phase in TJ-II. Moreover, with the recent recommissioning of a beam-based Charge Exchange Recombination Spectroscopy (CXRS) diagnostic, ion temperature profiles, as well as electron density and temperatures profiles, can now be compared for plasmas with and without PIs. This was done as it was considered that the majority ion temperature, T_i, measured using Neutral Particle Analysers, might not reflect the true central ion temperatures, T_{i0}, during a PiEC phase since high densities can result in significant attenuation of the flux of charge-exchange neutrals escaping from such a core [21]. Finally, pellet injections are performed into plasmas confined when the toroidal magnetic field direction is reversed. Since the same

NBI injector is used for both situations, the influence of NBI orientation on PiEC phase development can be evaluated. It is considered also that pellet radial deposition should be independent of toroidal B-field direction since the acceleration of ablated clouds that detach from a pellet should be independent of this direction [22]. Thus, these same injections allow this assumption to be substantiated. Finally, some comments are made with regard to current results and those from other stellarator devices and future plans for continued studies on TJ-II are outlined.

2. Experimental arrangement

TJ-II is a four-period low-shear heliac-type stellarator. It has major radius, R, $=$ 1.5 m, average minor radius, a, $\leqslant$0.22 m, plasma volume contained within the last-closed flux-surface (LCFS), $V_{\rm plasma}$, $\leqslant$1.1 m^3, and on-axis magnetic field, B_0, $\leqslant$1 T [8]. Plasma is created and heated with microwaves from 2 gyrotrons that operate at 53.2 GHz, the 2nd harmonic of the electron cyclotron resonance frequency ($P_{\rm ECRH} \leqslant$ 500 kW). With this electron cyclotron resonance heating (ECRH) system, plasma can be maintained for up to 300 ms and central electron densities, $n_{\rm e0}$, and temperatures, $T_{\rm e0}$, up to 1.7×10^{19} m^{-3} and 1.5 keV, respectively, are achieved, albeit not simultaneously. The corresponding central ion temperature, $T_{\rm i0}$, is $\sim$80 eV. Additional heating is provided by 2 tangential Neutral Beam Injector (NBI) systems that operate in a co-/counter-configurations (parallel/anti-parallel to the direction of the toroidal magnetic field) [23]. These provide up to $\sim$1 MW of through-port power at $\leqslant$32 keV into the vacuum chamber for $\leqslant$120 ms. As a result, $n_{\rm e0}$, $T_{\rm e0}$, and $T_{\rm i0}$ up to 5×10^{19} m^{-3}, 400 eV, and 130 eV, respectively, are achieved, again not simultaneously, when a boron plus lithium coating is applied to the inner vessel wall [24].

2.1. Pellet injector

A pipe-gun type pellet injector system is operated on TJ-II [25]. Although 4 pellets can be formed prior to a discharge, only 3 are available here due to technical issues. Cylindrical hydrogen pellets with diameters of 0.5 mm, 0.66 mm, 0.76 mm, and/or 1 mm and with lengths similar to diameters can be formed. Straight guide pipes direct them to the plasma outer edge for all cases. These are arranged so that flight paths for pellets exiting two of the guide tubes pass through the magnetic axis whereas the flight paths of the pellets exiting the two other tubes have nearest approach to the same magnetic axis at $\rho = \sim$0.35, where $\rho = r/a$ is normalized plasma radius and r is radius. In addition, the positions of the formation tubes of different diameters can be interchanged. In all cases, pellet velocities and masses are determined using light-gate and microwave cavity diagnostics positioned along the guide tubes. Although fast propellant valves and high gas pressures (65 bar) are used for pellet acceleration to high velocities (800–1200 m s^{-1}), jump gaps and vacuum expansion volumes minimize gas pressure build-up in the guide tubes as well as the quantity of gas that reaches the main vacuum chamber. Also, as this is a pipe-gun type injector, pellet firing times can be programmed prior to a discharge. This also allows pre-programming separation times between pellet arrival times. Finally, pellet ablation light is collected using fibre-optic cables fitted with narrowband interference filters (centred at 660 $\pm$ 2 nm). These are positioned on the airside of viewports located in the same machine sector and the fibres are connected to light-sensitive silicon diodes.

2.2. Diagnostics

TJ-II is equipped with a broad range of plasma diagnostics [26]. See figure 1. These include a Thomson Scattering (TS) system that provides a single set of $n_{\rm e}$ and $T_{\rm e}$ profiles ($0 \leqslant \rho \leqslant \sim$0.8) per discharge [27], a microwave interferometer that produces a trace of line-averaged electron density, $<n_{\rm e}>$, a diamagnetic loop that yields measurements of stored diamagnetic energy, $W^{\rm E}_{\rm diag}$ [28], Balmer Hα (656.3 nm) monitors, and a multi-foil soft x-ray system that allows measurement of central electron temperature, $T_{\rm e0}$, along the NBI-heated phase of discharges [29]. In addition, a two-channel Doppler Reflectometer (DR) system and a dual Heavy Ion Beam Probe (HIBP) system are available [30, 31]. The two-channel DR system is a dual-frequency hopping system (33–50 GHz, X-mode) with a probing beam angle range of $\pm$20° that provides measurements of $E_{\rm r}$ and turbulence dynamics at two selectable radial positions in the outer plasma region. The HIBPs, called HIBP#1 and HIPB#2, provide direct measurements of plasma potential, $\varphi(\rho)$ [32] and yield fluctuation measurements for plasma potential and density, $\tilde{n}_{\rm e}(t)$, the latter being proportional to measured fluctuations in the collected secondary beam current, $\tilde{I}_{\rm HIBP}$ [33]. With this set-up, one or both HIBP can be set to monitor at fixed radial positions with temporal resolution of 1 μs, or one or both can be set to scan continuously between the plasma inner and outer edges, typically once every 10–20 ms.

An important plasma parameter to consider in PiEC scenarios is ion temperature, $T_{\rm i}$. In the past, a Charge-Exchange Recombination Spectroscopy (CXRS) diagnostic had been available on TJ-II [34]. However, it was modified in 2014 to obtain Motional Stark Effect measurements [35], thus $T_{\rm i}$ profiles were not available for [9]. Here, it has been recommissioned for CXRS. With it, localized $T_{\rm i}$ measurements are obtained across the minor radius by injecting a 5 ms duration neutral beam pulse of hydrogen atoms accelerated to 30 keV into the plasma once per discharge (e^{-1} beam radius $=$ 21 mm). Light, emitted at $\sim$529 nm by the de-excitation of C^{+5} ions after C^{+6} ions have undergone charge exchange with beam neutrals, is collected by lenses and fibres located outside viewports located above and below the beam path through the plasma as well by a similar optical combination located in a nearby tangential access port. The shot-to-shot technique is used to separate background plus beam-stimulated C VI light from background C VI light and 28 lines-of-sight cover radial locations between $\rho = \sim$0.05 and $\sim$0.8. Finally, measured CXRS measurements are corrected, if necessary, for non-thermal fluctuations as the contribution of such fluctuations to Doppler-broadened line-widths can lead

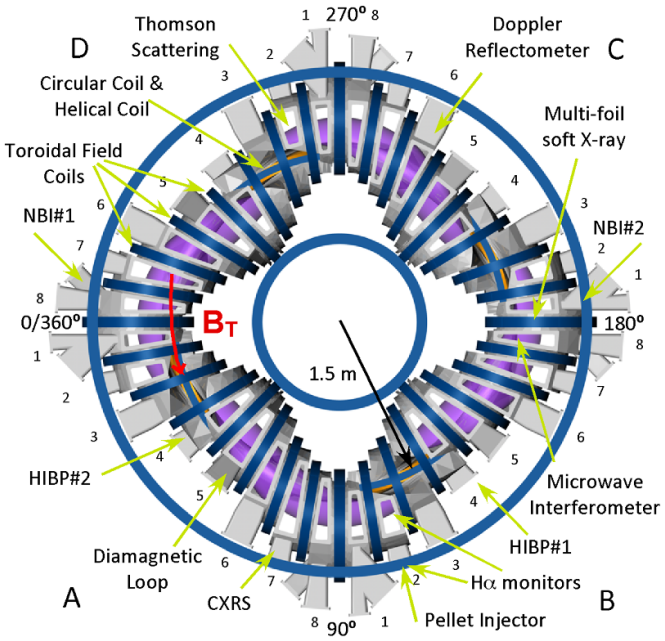

Figure 1. A bird's-eye view sketch of TJ-II showing locations of diagnostics of interest as well as quadrants A through to D, and sectors 1–8. The vacuum chamber is grey, magnetic field generation coils are dark blue (vertical, toroidal and circular) and orange (helical), and the plasma is purple. The device is operated nominally with an anti-clockwise toroidal magnetic field direction, B_T, when viewed from above.

to excess T_i values [36, 37]. Although the CXRS method measures impurity ion temperature, it was shown in [38] that good agreement is achieved between central majority (Neutral Particle Analyzer) and impurity (CXRS) ion temperatures in TJ-II.

2.3. Experiment set-up

In this work, up to 3 hydrogen pellets are injected in sequence into the NBI-heated phase of TJ-II discharges that are confined using magnetic configurations 100_44_64 ($a = 0.1925$ m, $\iota_0/2\pi = 1.55$, $V_{plasma} = 1.098$ m^3) or 100_48_65 ($a = 0.191$ m, $\iota_0/2\pi = 1.591$, $V_{plasma} = 1.09$ m^3) where $\iota_0/2\pi$ is the on-axis rotational transform and $B_0 = 0.95$ T. See, for instance, figure 1 of [39]. The configuration label 'xxx_yy_zz' refers to currents in the circular, helical, and vertical field coils, respectively, of this current-free stellarator. In TJ-II, its magnetic trap is achieved using several sets of coils that determine completely the magnetic surfaces before plasma discharge initiation. For this, its toroidal field is created by 32 coils, termed toroidal field coils, whilst the 3-dimensional twist of the central axis of the configuration is created by means of 2 central coils: 1 circular coil plus 1 helical coil. Next, the vertical plasma position is controlled by vertical field coils. Finally, the combined action of these magnetic fields generates the bean-shaped magnetic surfaces. As noted, plasma, with hydrogen as the working gas, is created using ECRH. Once developed, additional heating provided by one or both NBIs maintains the plasma and ECRH is switched-off. In all discharges here, the gas-puff is closed just prior to NBI start-up. Now, if a pellet containing $>\sim10^{19}$ H atoms is injected during the NBI phase of a discharge, some ice will penetrate beyond the magnetic axis due to the low electron temperature, *i.e.* $\leqslant$400 eV [17, 40]. Also, if a pellet contains $<\sim2.5 \times 10^{19}$ H atoms then the ice is typically burnt out before reaching the inner plasma edge. In contrast, a larger pellet may not be fully burnt out when traversing the plasma so excess ice will exit the plasma. However, since a strong outward radial drift generally occurs for detached pellet clouds at all radii in this device, a significant fraction of pellet particle deposition will occur within the region $\rho \leqslant 0.6$ [9, 16, 41]. In addition, pellet injection results in a strong T_{e0} reduction in the central plasma region as well as in a significant step-like increase in $<n_e>$. In the case of NBI-heated plasma, T_{e0} recovers to pre-injection values within a couple of milliseconds [17]. In the experiments undertaken here, pre-programmed time-gaps between sequential fast-valve openings are from 5 ms to 15 ms. Such values are chosen as they mirror post-injection energy confinement times for PiEC phases in TJ-II reported previously [9].

3. Experimental description and results

As noted, a PiEC phase is observed after the injection of a single hydrogen pellet with $>10^{19}$ H atoms into the NBI-heated phase of a TJ-II discharge. Indeed, such a phase exhibits clear increases in stored diamagnetic energy and energy confinement once the ablated pellet material has been homogenized about the plasma. Moreover, a single heating beam is capable of maintaining this PiEC phase until beam switch-off, *i.e.* typically 50 ms after PI. In many cases, the duration of such a PiEC phase represented several confinement times. When experimental energy confinement times were compared with predictions made using the ISS04 Scaling law for TJ-II [18, 19], improvements of up to 40% were observed for post-injection $<n_e>$ between 2.5×10^{19} and 3.5×10^{19} m^{-3} [9]. In addition, a bifurcation was observed in [9]. when plots of the triple product, $n_e \cdot T \cdot \tau_E{}^{diag}$, versus time along the discharge were compared for discharges with and without a PI. Here, $\tau_E{}^{diag}$ is experimental energy confinement time and a bifurcation is understood to be a significant long-lasting change (improvement) of confinement properties during which the external system drive (NBI heating) remains unchanged. Given that only a single PI was performed for the discharges presented, it was considered that PiEC plasma parameters were well within TJ-II operational limits. Here, multi-pellet injections are performed in order to explore some of these boundaries in TJ-II. Finally, TJ-II is usually operated with its toroidal B field in the anti-clockwise direction when viewed from above, see figure 1. A short experimental campaign with a reversed B field was undertaken recently, thus an experiment was performed to compare post-injection PiEC performances for both set-ups when using the same NBI heating beam. The findings from these experiments are presented in the following subsections.

3.1. Multi-pellet injections

Experiments are performed here in discharges maintained using NBI heating. In the first instance, a pellet is injected initially to induce a PiEC phase and, later, additional pellets are injected to further enhance this phase. Time traces from a range of diagnostics are subsequently analysed in order to elucidate on the plasma response and to determine how parameters such as W^{E}_{diag} and $\tau_E{}^{diag}$ evolve along such discharges.

In figure 2, selected time traces for TJ-II discharges with and without PIs are shown. First, in figure 2, $<n_e>$, T_{e0}, Balmer Hα, W^{E}_{diag}, $\tau_E{}^{diag}$ and $\tau_E{}^{ISS04}$ traces are plotted for reference plasma, #52580. This discharge is created using the 100_44_64 configuration and with ECRH power only. Then, once established, 400 kW of through-port power is injected into the vacuum chamber using the counter-NBI system (NBI#2) and ECRH power is switched-off. Next, in figure 2, a single pellet containing 1.1×10^{19} H atoms is injected during the NBI-heated phase of discharge #52588. This single pellet induces a step-like increase in $<n_e>$, a transient decrease in T_{e0}, as well as abrupt reductions in well-developed Hα fluctuations, which can be associated with ELM-like modes in TJ-II [42], and in Mirnov coil fluctuations [40]. The latter, *i.e.* abrupt reductions in Mirnov coil fluctuations, begin before pellet particle homogenization is completed, *i.e.* $\leqslant$0.5 ms after pellet entry into the plasma, and remain reduced for several milliseconds. These are associated with the concurrent abrupt decrease in T_e. In addition, W^{E}_{diag} is observed to increase steeply at ~0.5 ms after PI. Then, as #52588 progresses, the slope of W^{E}_{diag} begins to flatten when it reaches ~3 kJ, this flattening coinciding with the redevelopment of Hα activity (at ~30 kHz). Thereafter, the temporal evolution of W^{E}_{diag} mirrors that of reference discharge #52580, before finally reaching a maximum of 3.6 kJ at NBI switch-off. In contrast, in #52580, W^{E}_{diag} increases steadily up to ~3 kJ at NBI switch-off, this reference discharge having a L- to H-mode like transition at ~1207 ms [43]. This value of ~3 kJ is representative of the maximum W^{E}_{diag} that has been achieved in TJ-II with a single NBI and a lithium-coating recently applied to the wall [44]. Finally, TS data are plotted for these discharges in figure 3. It is seen that the PI causes a ~50% increase in n_{e0}, when compared to #52580, and in more negative density gradients across almost the full plasma minor radius. In contrast, T_e is reduced inside $\rho = 0.3$, the reduction in T_{e0} being less than ~20%. The tendencies observed here are representative of the PiEC phase described in [9] where only single pellet injections were performed.

In a second example, discharge #52586, 3 pellets are injected in sequence. See figure 2. The first pellet contains ~1.4×10^{19} H atoms, while the other two contain ~5×10^{18} H atoms each. The time separations are ~13.5 ms, these separations being comparable with PiEC phase energy confinement times [9]. Again, $<n_e>$ shows a step-like increase after each PI, the step size depending on pellet content. Also, the first PI subdues well-developed ELM-like H_α fluctuations and again W^{E}_{diag} rises steeply before flattening out as H_α fluctuations begin to reappear. Thereafter, the 2nd and 3rd pellets induce further, albeit smaller, rises in W^{E}_{diag}, which reaches ~4 kJ. A notable effect of the 2nd and 3rd pellets, which travel along flight paths that have nearest approach to the magnetic axis at $\rho = 0.34$, is a broadening of the density profile (n_{e0} is almost unaffected by the additional pellets) with the result that the density gradient become more negative outside $\rho = 0.7$ when compared to #52588 (1 PI). See figure 3(*c*). In contrast, the impact of these pellets on T_{e0} is minimal.

A clear characteristic of the TJ-II PiEC phase reported in [9] that is reproduced here during the post-PI injection phases of #52586 and #52588, is a significant increase in the energy confinement time, τ^{E}_{diag}. Here, $\tau_E{}^{diag}$ is estimated as $\tau_E{}^{diag} = W^{E}_{diag}/(P_{abs} - dW^{E}_{diag}/dt)$, where absorbed NBI power, P_{abs}, which is plasma density dependent [45], is evaluated using the FAFNER2 code that considers charge exchange, fast-ion and shine-through losses [46, 47]. It should be noted that deviations between calculations, based on experimental density and temperature profiles, and values predicted by FAFNER2 fits for P_{abs} are of the order 10% to 15%. Next, in relation to comparisons with $\tau_E{}^{ISS04}$ predictions, it should be noted that the renormalization factor employed in [9] and here for $\tau_E{}^{ISS04}$ is not the original TJ-II renormalization factor of 0.25 which was quoted in [18] for boron-coated wall ECRH discharges. This is because in the comparative study reported in [44] for boron-coated wall and lithium-coated wall discharges, it was proposed that a renormalization factor larger than 0.25 is needed when lithium-coated wall NBI discharges are considered. Later, in [19], a revised renormalization factor of 0.5 was defined for such cases. This latter factor is used here. Hence, the ISS04-based Scaling law used hereafter in this paper is given by

$$\tau_E{}^{ISS04} = 0.5 \cdot \left(0.134 \cdot a^{2.28} \cdot R^{0.64} \cdot P_{abs}{}^{-0.61} \cdot < n_e >^{0.54} \cdot B^{0.84} \cdot \iota_{2/3}{}^{0.41} \right) \quad (1)$$

where a, R, $<n_e>$ and B are defined in section 2, P_{abs} is absorbed NBI power (MW), and $\iota_{2/3}$ is the rotational transform at $\rho = 2/3$. Next, following these definitions, $\tau_E{}^{diag}$ and $\tau_E{}^{ISS04}$ values at maximum W^{E}_{diag} are compared in table 1 for the discharges of interest here. It is seen that the confinement enhancement factor, $\tau_E{}^{diag}/\tau_E{}^{ISS04}$, is close to 1.08 for the reference discharge but increases to 1.18 and 1.29 for the discharges with one and three pellet injections, respectively. A second parameter shown in this table is the density peaking factor, *i.e.* the quotient between central electron density, as measured by TS, and line-averaged density. This increases significantly after the injection of a single large pellet, *i.e.* from 1.28 for #52580 (no PI) to 1.72 for #52588 (1 pellet). However, the injection of the additional smaller pellets results in reduced peaking factor values, *i.e.* from 1.72 for #52588 to 1.4 for #52586. This is because pellet material is deposited at outer ρ rather at ρ close to the magnetic axis.

In summary, a cryogenic pellet, containing >~10^{19} H atoms, injected into a counter NBI-heated discharge in TJ-II gives rise to a PiEC phase in which W^{E}_{diag} and $\tau_E{}^{diag}$ values are significantly larger than predicted W^{E}_{ISS04} and $\tau_E{}^{ISS04}$ values. Injections of additional small pellets induce further increases in W^{E}_{diag} and $\tau_E{}^{diag}$, the former reaching values that

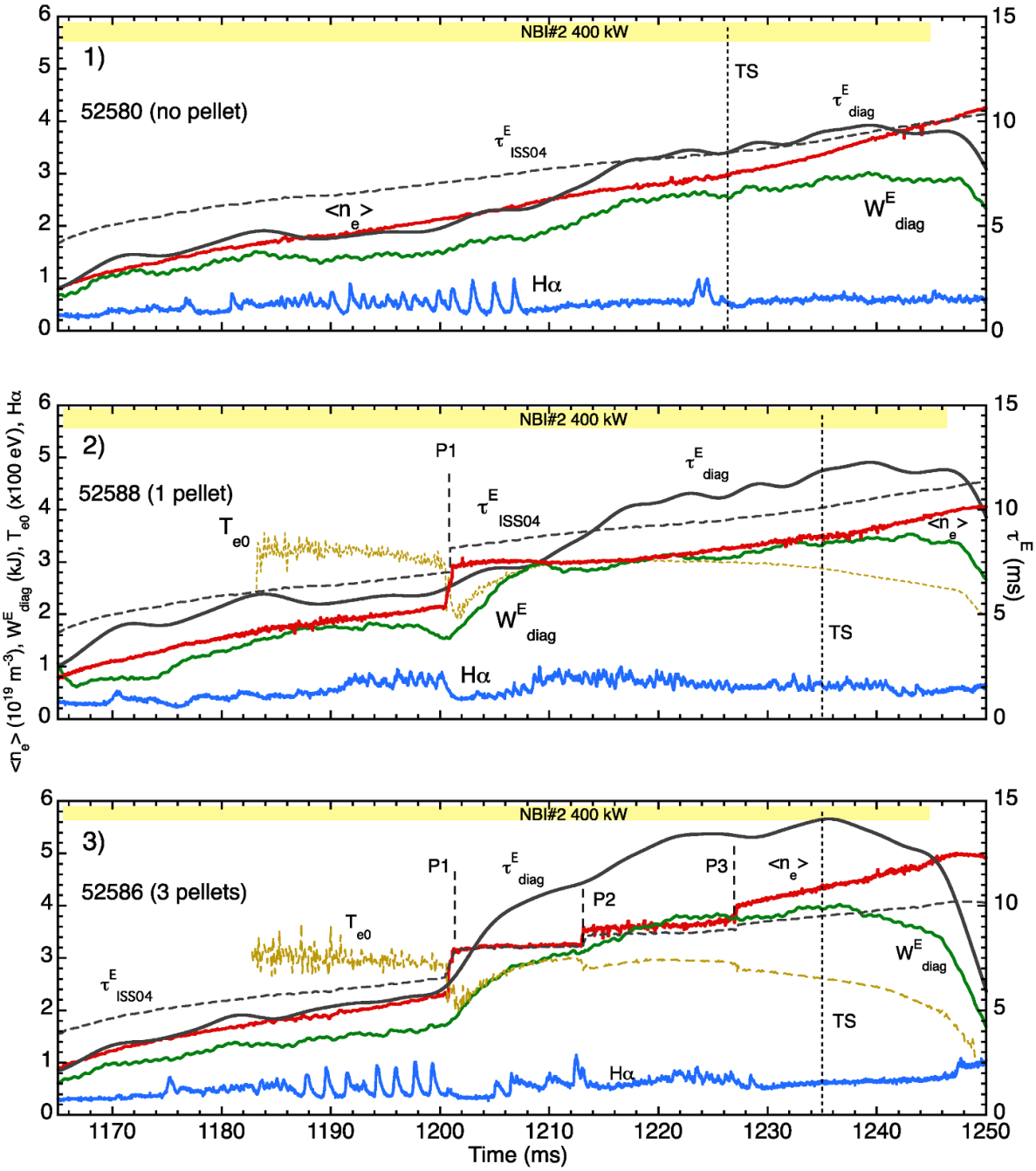

Figure 2. Time traces for discharges (1) #52580 (no pellet), (2) #52588 (1 pellet) and (3) #52586 (3 pellets). 430 kW of ECRH is injected from 1060 ms until 1160 ms and 400 kW of through-port power is injected by NBI#2 between 1140 ms and 1245 ms. A single pellet with $\sim 1.1 \times 10^{19}$ H atoms is injected at $\sim$1200 ms of #52588. Three pellets, with $\sim 1.4 \times 10^{19}$, $\sim 5 \times 10^{18}$ and $\sim 5 \times 10^{18}$ H atoms, are injected at $\sim$1200 ms, $\sim$1213 ms and $\sim$1236 ms of #52586. Signals are line-averaged electron density (red), stored plasma diamagnetic energy (green), Balmer Hα emission (blue), T_{e0} (olive dash-dash), τ_E^{ISS04} (black dash-dash) and τ_E (black). T_{e0} is not available for 52580.

are unattainable for similar plasma conditions fuelled by gas-puff and/or recycling. Additionally, these discharges are maintained until NBI switch-off.

3.2. Ion temperature profiles

An important plasma parameter to consider for PiEC scenarios is ion temperature, T_i. In order to determine how PIs affect ion temperature in TJ-II, TS and CXRS are compared for a reference discharge, #55511, and for a similar discharge with PI, #55313. For this, a single pellet containing 2.3×10^{19} H atoms is injected into the NBI-heated phase of discharge #55313 which is created using configuration 100_44_64. See figure 4 where time traces of $<n_e>$ and W^E_{diag} are plotted for these discharges which are heated by 450 kW of through-port power from NBI#2. As before, PI leads to an abrupt jump in $<n_e>$ and a rapid rise in W^E_{diag} which reaches a plateau that continues until NBI switch-off. Next, TS and CXRS profiles

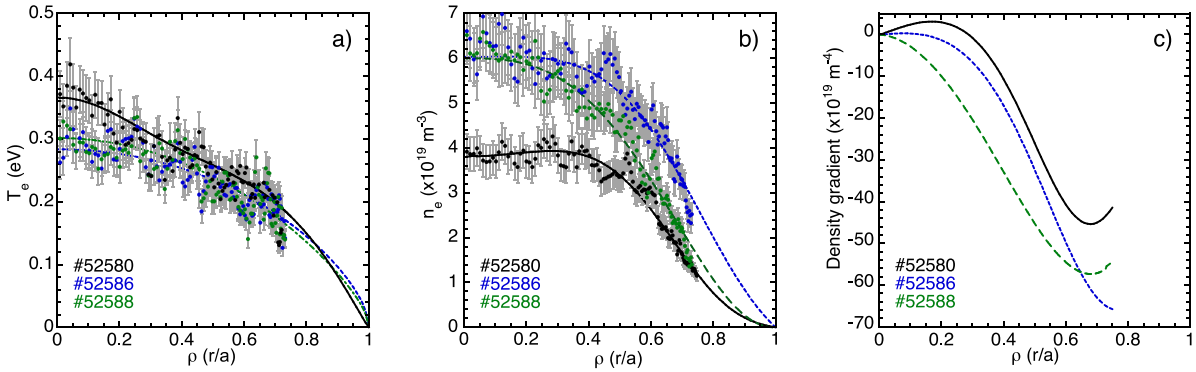

Figure 3. (*a*) TS data points for T_e plus fitted curves for #52580 (black), #52588 (green) and #52586 (blue). (*b*) TS data points for n_e plus fitted curves with the same colouring for the discharges. The TS is set at 1226.4 ms for #52580 and at 1235 ms for the other discharges. (*c*) Density gradient versus normalized radius with the same colouring scheme used for the discharges in (*a*) and (*b*). In this case, the graphs are limited to inside $\rho = 0.75$ where experimental data points are available.

Table 1. Summary of plasma parameters for discharges described in section 3.1. N_{e0} and T_{e0} are obtained using TS, thus $n_{e0}/<n_e>$ is estimated when measurements are made. $\tau_E{}^{diag}$ and $\tau_E{}^{ISS04}$ values are taken when $W^E{}_{diag}$ is maximum along each discharge.

Discharge	Number of pellets	N_{e0} (10^{19} m^{-3})	T_{e0} (eV)	$n_{e0}/<n_e>$	$W^E{}_{max}$ (kJ)	$\tau_E{}^{diag}$ (ms)	$\tau_E{}^{ISS04}$ (ms)	$\tau_E/\tau_E{}^{ISS04}$
52580	0	3.8	370	1.28	3	10.5	9.7	1.08
52588	1	6.0	300	1.72	3.6	12.25	10.4	1.18
52586	3	6.0	280	1.4	4	14.1	10.9	1.29

are compared in figure 5 for these discharges which are selected as their line-averaged densities are similar when these measurements are performed, *i.e.* $<n_e> = 4.5 \times 10^{19}$ m^{-3} for #55511 (reference) and $<n_e> = 4.235 \times 10^{19}$ m^{-3} for #55313 (PI). In contrast, $W^E{}_{diag} = 2.9$ kJ for #55511 and $W^E{}_{diag} = \sim 3.6$ kJ for #55313 (PI). It should be noted that the 2.9 kJ of stored diamagnetic energy is representative of the highest $W^E{}_{diag}$ achieved for counter-NBI heated plasmas in TJ-II with a lithium-coated wall [19, 44]. Finally, the plots in figure 5 reveal that whilst T_{e0} and n_{e0} and their profiles are similar for both discharges, T_{i0} increases by ∼45% after PI, *i.e.* from ∼115 eV for #55511 to ∼165 eV for #55313. Indeed, significantly higher T_i values are seen at all radii inside $\rho = 0.8$, the outer radial limit for CXRS measurements. The findings would indicate that the additional diamagnetic energy in #55313 is stored mainly in the ion channel rather than in electron channel.

In a second example (see figure 6), 2 pellets containing 2×10^{19} and 1.4×10^{19} H atoms are injected into discharge #55300 which is also heated by 450 kW of through-port power from NBI#2. Again, each injection leads to an abrupt jump in $<n_e>$ as well as to a rise in $W^E{}_{diag}$ that continues until $W^E{}_{diag}$ reaches a maximum of ∼4.4 kJ for $<n_e> = \sim 6 \times 10^{19}$ m^{-3}. The subsequent fall in $W^E{}_{diag}$ indicates that the discharge is no longer sustained and that some density/power limit is reached. Next, TS and CXRS profiles for this discharge, made when $W^E{}_{diag} = \sim 4.4$ kJ, and for discharge #55511 are compared in figure 7. In these profiles, T_{e0} reduces from ∼325 eV for #55511 to ∼285 eV for #55300, whereas n_{e0} and T_{i0} increase by ∼50% and ∼60%, respectively, *i.e.* from $\sim 6 \times 10^{19}$ m^{-3} and ∼115 eV for #55511 to $\sim 9 \times 10^{19}$ m^{-3} and ∼185 eV for #55300. These findings confirm that as additional cryogenic pellets are injected into TJ-II the electron density and ion temperature continue to increase until density reaches an upper limit. In contrast, a slow decay in electron temperature is observed as additional pellets are injected. These findings will be discussed in more detail in section 4.

3.3. PIs into reversed-B field plasmas

TJ-II is operated normally with its toroidal magnetic field orientated in the anti-clockwise direction when viewed from above the device. See figure 1. This direction is preferred as the HIBP systems are designed for such a field direction. Nonetheless, experiments are occasionally performed with a reversed B-field direction, *i.e.* B follows a clockwise direction when viewed from above. For instance, during 2023, a short experimental campaign was undertaken with a reversed-B field during which some PI experiments were performed. For this, it is necessary to invert the currents in all field coil sets. Some technical issues with the NBI#1 system limited additional heating to NBI#2 only, thus NBI#2 operated in co-counter configuration (parallel to the toroidal magnetic field direction). Thus, an experiment was performed to determine if the PiEC phase achieved in TJ-II using counter-NBI heating, see sections 3.1 and 3.2, could be reproduced using co-counter NBI heating with the same beam operational parameters. As an addendum, the experiment allows comparison of particle deposition profiles for pellet injections performed into clockwise and anti-clockwise B fields. Such an experiment can confirm if the acceleration of detached plasmoids, $\delta V_d/\delta t = 2(P_0 - P_\infty)/(L_B\ N_0\ m_i)$, is independent of B field

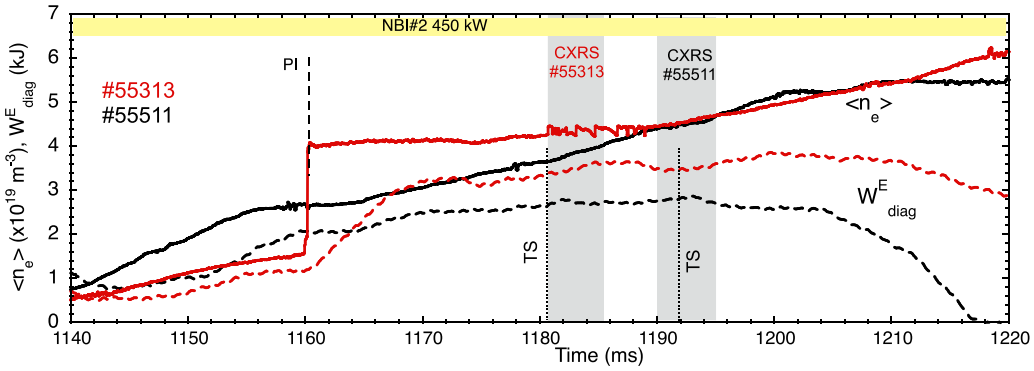

Figure 4. Time traces of line-averaged density (continuous) and stored diamagnetic energy (dash-dash) for TJ-II discharges, #55511, without PI (black), and #55313, with PI at 1160 ms (red). TS (vertical dot-dot) and CXRS (shaded grey) are performed when the line-averaged densities in both discharges are close to 4.4×10^{19} m^{-3}.

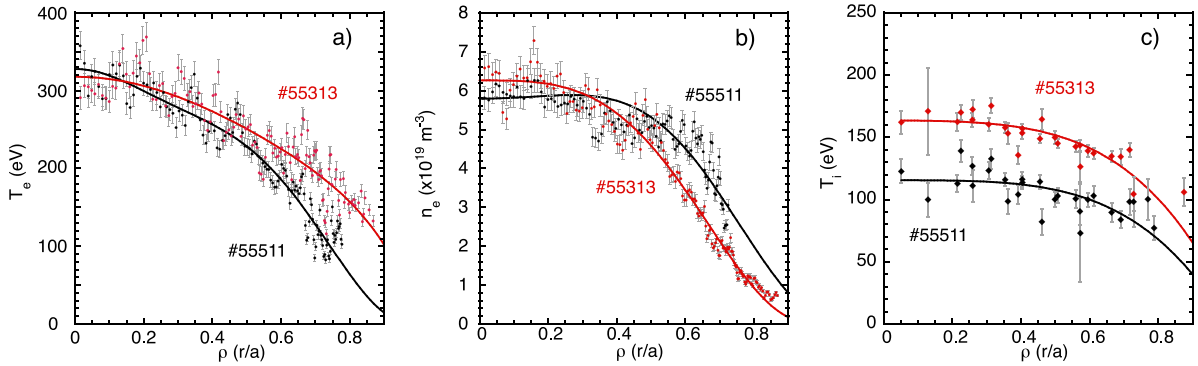

Figure 5. (*a*) TS data plus fitted curves for T_e taken at 1195 ms of discharges #55511 (black) and at 1182 ms of #55313 (red). (*b*) TS data plus fitted curves for n_e with the same colouring for the discharges. (*c*) T_i profiles measured between 1190 ms and 1195 ms of #55511 and between 1182 ms and 1187 ms of #55313 using CXRS with the same colouring for the discharges.

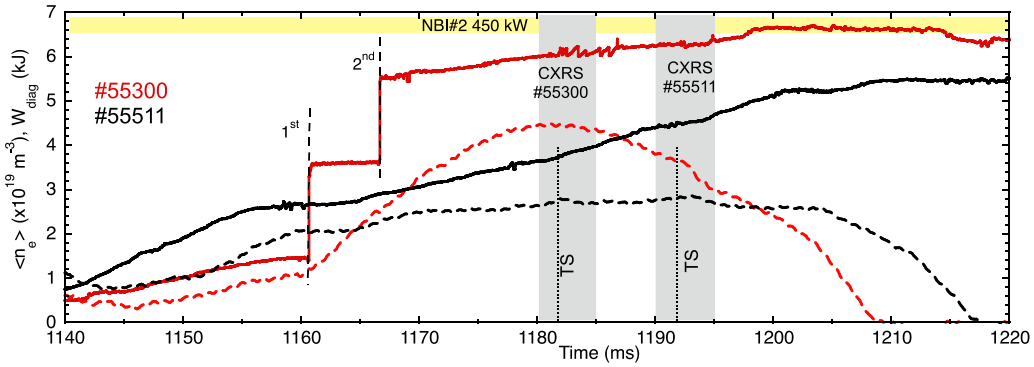

Figure 6. Time traces of line-averaged density (continuous) and stored diamagnetic energy (dash-dash) for TJ-II discharges #55511, without PIs (black), and #55300, with PIs at 1160 ms and 1166 ms (red). The NBI heating interval and the instances when TS (vertical dot-dot) and CXRS (shaded grey) are performed are highlighted.

direction [22]. Here P_0 and P_∞ are plasmoid and plasma pressures, $L_B = B_\infty/\nabla_\perp B_\infty$, the magnetic cross-field gradient scale-length, where ${L_B}^{-1}$ is close to $+1$ m^{-1} in TJ-II [3], N_0 is plasmoid density and m_i is ion mass.

In the experiment, 2 pellets are injected per discharge into similar target plasmas contained using the normal (#55300 discussed in section 3.2) and reversed-B field (#55240) directions. For these, the standard 100_44_64 configuration is employed and after an initial ECRH phase, plasmas are maintained and further heated with 450 kW of through port power from NBI#2. All standard diagnostics, except the HIBP system for the reversed-B field case, are available as are dedicated pellet ablation instruments, *i.e.*, silicon diodes fitted with Balmer H_α filters and a fast-frame imaging camera that images pellet ablation and plasmoid drifting [16]. With the latter system it is observed that detached plasmoids drift outwards and

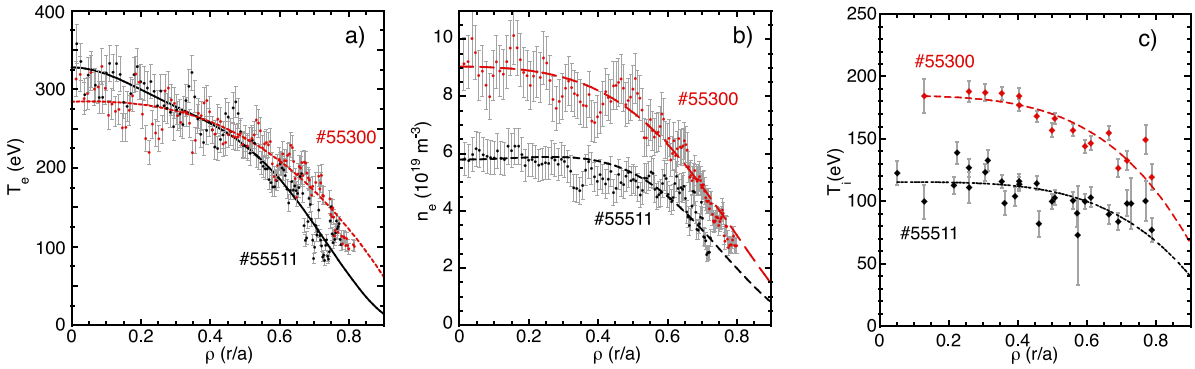

Figure 7. (*a*) TS data plus fitted curves for T_e obtained at 1182 ms for #55300 (red) and at 1190 ms for #55511 (black). (*b*) TS data plus fitted curves for n_e with the same colouring for the discharges in (*a*). (*c*) T_i profiles measured between 1180 ms and 1185 ms by CXRS for #55300 and from 1190 ms to 1195 ms for #55511. The same identification colourings are used here.

downwards for both B field directions, thus confirming the supposition noted previously. Next, in figure 8, time-traces of line-averaged densities and stored diamagnetic energies are plotted for these discharges. In both cases, the 1st pellet is injected at ∼1159 ms and follows a flight path that intercepts and penetrates beyond the magnetic axis, while the 2nd pellet is injected at 1167 ms and penetrates the full plasma without intercepting the magnetic axis. The pellets contain between 1.4×10^{19} and 2×10^{19} H atoms. The similar time traces seen in figure 8 for $<n_e>$ and W^E_{diag} both before and after the PIs indicate that the development and maintenance of a PiEC phase by cryogenic PIs is independent of B field toroidal direction and of counter or co-counter NBI heating in the TJ-II. This is confirmed by the similar post-injection T_e, n_e and T_i profiles plotted in figure 9. It should be noted that the n_e profile is broadened radially for #55300 while T_i values are slightly higher for the same discharge, these differences being attributed to a slightly larger 2nd pellet in #55300.

3.4. Injection of largest pellets

In a final example, the largest available TJ-II pellets are injected in sequence into the NBI-heated phase of discharge #53685 (through-port power for NBI#2 = 480 kW), created using the 100_48_65 configuration and nominal-B field direction. This is done to investigate plasma parameter limits after large pellet injections into TJ-II. For this, 3 pellets with $\sim 3.5 \times 10^{19}$, $\sim 1.7 \times 10^{19}$ and $\sim 1.4 \times 10^{19}$ H atoms are injected with ∼10 ms separations (content of pellets = 6.6×10^{19} H atoms), these separations being comparable with post-injection $\tau_E{}^{diag}$ values. See figure 10 where time traces for $<n_e>$, T_{e0}, Balmer Hα, W^E_{diag}, and P_{rad} (total radiated power) are plotted. In the plots, W^E_{diag} reaches a maximum of 4.2 kJ when $<n_e> = \sim 6.1 \times 10^{19}$ m^{-3}. Thereafter, $<n_e>$ remains fairly constant while W^E_{diag} and T_{e0} decay slowly, the former returning to zero before NBI switch-off with a decay comparable to the confinement time. In addition, TS profiles, obtained when W^E_{diag} is maximum, show $n_{e0} = 1.2 \times 10^{20}$ m^{-3} and $T_{e0} = 175$ eV. See figure 11. Here, the n_{e0} value is amongst the highest achieved to date in TJ-II whilst the stored diamagnetic energy achieved, 4.2 kJ, is representative of the highest achieved after PIs into plasmas heated by a single NBI beam. The 4.2 kJ achieved also reflects a ∼25% improvement compared to maximum W^E_{diag} achieved in [19] without PIs for $<n_e>$ close to 6×10^{19} m^{-3}. At that time in [19], a liquid-lithium limiter (LLL) was employed. It resulted in marked reductions in impurities for TJ-II plasmas which have strong vacuum vessel wall interactions [48]. However, the LLL is not available here. In previous studies when lithium over boron wall coatings were employed, plasmas with W^E_{diag} up to 3.2 kJ for $<n_e>$ up to 4.8×10^{19} m^{-3} were attained when using a single NBI beam (NBI#2) [44]. Thus, the results reported here represent ∼30% improvements for both W^E_{diag} and $<n_e>$. In summary, the n_{e0} and W^E_{diag} achieved in discharge #53685 (3 PIs) are representative of the highest such values attained to date for TJ-II plasmas with PIs. The limits reached in terms of plasma density, temperature, energy and β, and the possibilities to extend these limits, are discussed in more detail in section 4.4.

4. Analysis and discussion

It is apparent from experiments on the TJ-II stellarator that the injection of pellet(s) enables new operational regimes to be reached in this device. For instance, it was reported in [9] that the injection of a single cryogenic pellet with $>10^{19}$ H atoms into a well-established NBI-heated plasma pushes the discharge into an enhanced confinement phase which can be maintained until beam switch-off. It has been shown here that the injection of additional pellets enables higher peak values of W^E_{diag} and longer $\tau_E{}^{diag}$ to be reached that those attained with a single PI. Moreover, the injection of the largest available pellets has allowed previously unachievable W^E_{diag} values to be reached for counter-NBI heated plasmas in TJ-II. In addition, CXRS measurements of T_i with/without PI(s) suggest increased collisional coupling between thermal electrons and ions and indicate that the ion contribution to the total plasma energy may be modified significantly. It was also noted in [9] that a PI results in increased central plasma beta, β_0, and normalized plasma, β, and it was postulated then that even higher values could be achieved after multiple PIs as the discharges investigated were not terminated by radiation collapse. These

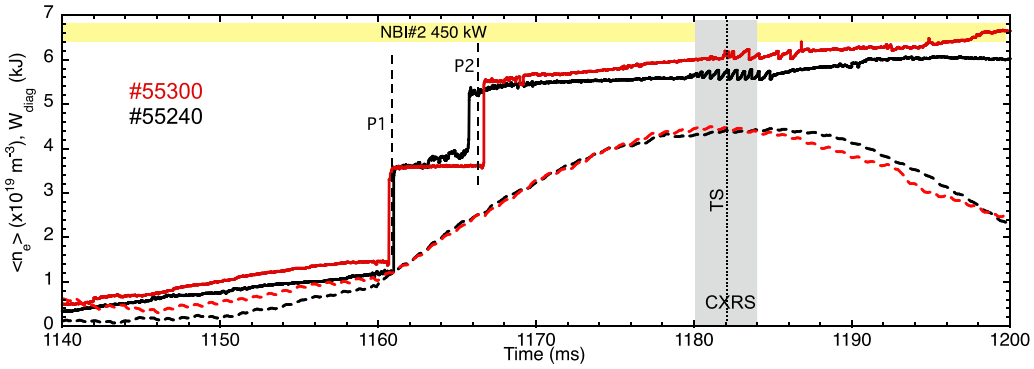

Figure 8. Time traces of line-averaged density (continuous) and stored diamagnetic energy (dash-dash) for two TJ-II discharges into which 2 cryogenic pellets are injected, #55300 (red) with nominal toroidal B field and #55240 (black) with reversed toroidal B field. The NBI heating interval and the instances when TS and CXRS are performed are highlighted.

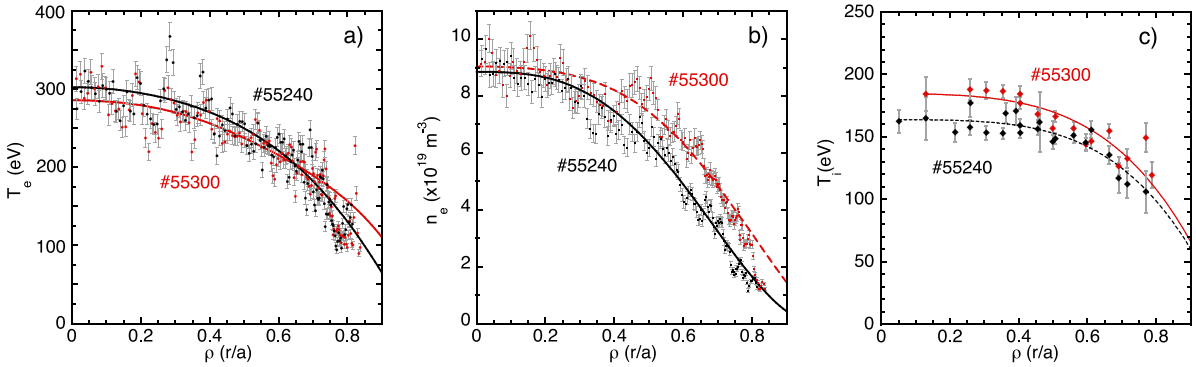

Figure 9. (*a*) TS data plus fitted curves for T_e obtained at 1182 ms for discharges #55300 (red) and #55240 (black) after the injection of cryogenic pellets at 1160 ms and 1166 ms. (*b*) TS data plus fitted curves for n_e with the same colouring for the discharges in (*a*). (*c*) T_i profiles measured from 1180 to 1185 ms using CXRS in which for same identification colourings are used for the discharges.

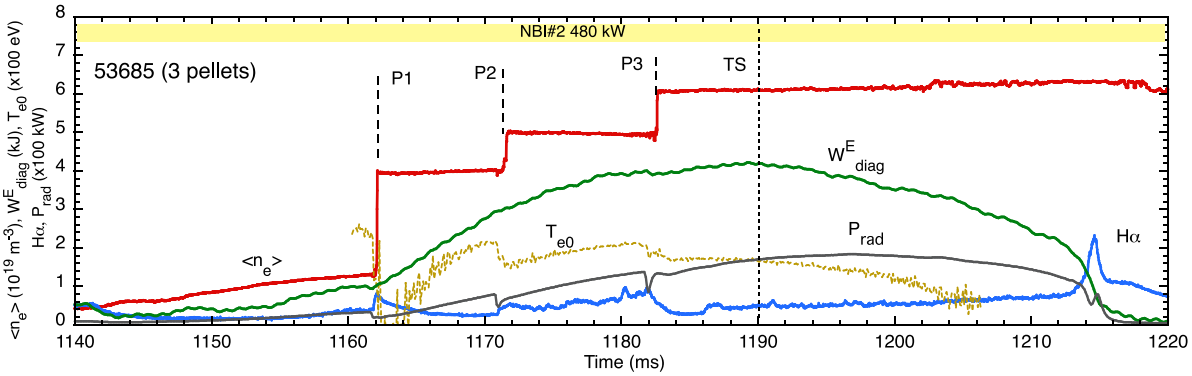

Figure 10. Time traces of selected signals along TJ-II discharge #53685. 480 kW of ECR heating is provided from 1060 ms to 1140 ms and 480 kW of NBI#2 through-port power is injected from 1120 ms to 1220 ms. Three pellets containing $\sim 3.5 \times 10^{19}$, $\sim 1.4 \times 10^{19}$ and $\sim 1.7 \times 10^{19}$ H atoms are injected at $\sim$1162 ms, 1171 ms and 1182 ms. Signals are line-averaged electron density (red), stored plasma diamagnetic energy (green), Balmer Hα emission (blue), central electron temperature (dash-dash olive) and radiated power (dark grey).

parameters and scenarios will be quantified and discussed in the following sub-sections.

4.1. Plasma thermal and diamagnetic energies

It is instructive to consider plasma thermal and diamagnetic energy contents for selected discharges in order to, for instance, determine how the ion contribution to the total thermal energy content is modified by pellet injections or establish to what extent the relative difference between thermal and diamagnetic energy content is modified by PI(s). Here, plasma thermal energy content, W^{E}_{th}, is obtained by integration of TS profiles to obtain the electron energy contribution and by integration of CXRS ion temperature profiles and ion density profiles, the latter based on TS electron density profiles corrected using Z_{eff} values, to obtain the ion

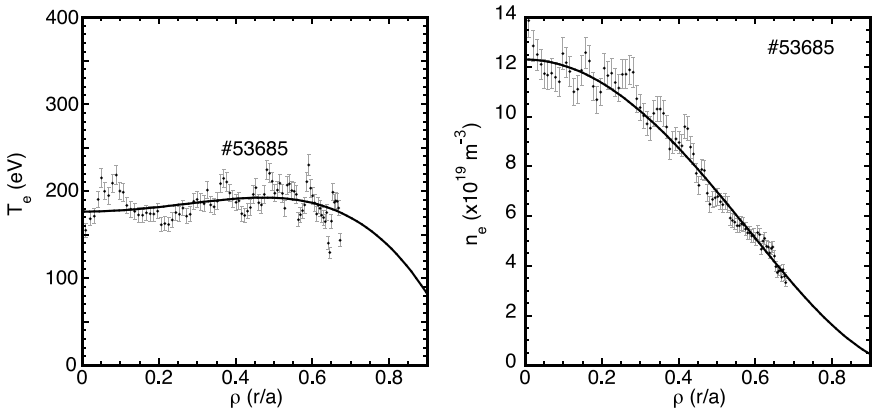

Figure 11. Thomson Scattering T_e and n_e profiles obtained at 1190 ms of discharge #53685.

contribution [49]. For this, it is assumed that electron and ion density radial profile shapes are similar, with profile scaling for ions based on experimental Z_{eff} values. As noted previously, it is assumed that majority ion and impurity ion temperatures are similar [38]. In the case of TS profiles, a reliable calibration of n_e values is made using the line-integrated electron density obtained with the microwave interferometer. Also, since the TS and CRXS diagnostics are limited to inside $\rho = 0.8$, n_e and T_e edge contributions are approximated out to the normalized effective plasma radius, $\rho = 1$, using parabolic dependences [44].

As an example, in discharges #55511 (no PI), #55313 (1 PI) and #55300 (2 PIs) of figures 4–7 the ion contribution rises from 30% to 36.6% and 41.5%, respectively. Here, $Z_{eff} = 1.4$ for #55511 and $Z_{eff} = 1.1$ for #55313 and #55300 in the time periods when W^E_{diag} is maximum. Z_{eff} is measured here using soft x-ray traces and assuming carbon as the main impurity. In a previous study of this ratio in TJ-II [44], the ionic share of the thermal energy for an NBI-heated plasma with Li-coated walls and $Z_{eff} = 1.5$ was determined to be around 30%, thus the present value when no PIs are performed is consistent with previous values. In contrast, the injection of pellets causes the ion contribution to increase significantly, as noted here. These ratios reenforce the hypothesis of increased collisional coupling between thermal electrons and ions after PIs as mentioned in section 3.2.

Stored diamagnetic energy values are extracted from data collected by diamagnetic loops installed inside the TJ-II vacuum vessel [28, 50]. The relative differences between thermal and diamagnetic energies, estimated as $(W^E_{diag} - W^E_{th})/W^E_{diag}$, can be determined here for the discharges selected in the previous paragraph. For the discharge without PI, this difference is 0.24 for #55511 (at $<n_e> = 4.4 \times 10^{19}$ m^{-3}). For discharges with PIs, the values are 0.36 for #55313 (1 PI and $<n_e> = 4.4 \times 10^{19}$ m^{-3}) and 0.073 for #55300 (2 PI and $<n_e> = 6.2 \times 10^{19}$ m^{-3}). In [44], relative differences were plotted for a range of $<n_e>$ and for different NBI set-ups. It was found then that relative differences decrease with increasing density. Such differences may be attributed to contributions by non-thermal particles to the energy content measured by the diamagnetic loops, *e.g.*, from fast-ions. Indeed, the fast-ion population should be inversely proportional to plasma density. Although a similar tendency occurs here, it cannot be confirmed with certainty. However, the relative differences for #55511 (no PI) and #55313 (1 PI), which have similar line-averaged densities, are 0.24 and 0.36, respectively. Finally, the 7.3% difference found at the highest density reviewed here, *i.e.* at 6.2×10^{19} m^{-3} in #55300, may be attributable to experimental uncertainties in TS and CXRS profiles, as well as in diamagnetic loop measurements, though it might also reflect the existence of a small residual fast-particle population.

4.2. Plasma β

It is instructive also to consider plasma beta, in particular how β is modified by PI(s) and what upper limits can be reached for current TJ-II operational conditions. Before presenting PI examples, it is useful to first consider β values for a reference discharge that reaches a W^E_{diag} value close to the maximum achievable without PI when using counter-NBI heating in TJ-II [19], *e.g.* discharge #55511 of figure 6 where maximum W^E_{diag} is ∼3 kJ. In this case β_0 and β are obtained between 1190 ms and 1195 ms, *i.e.* $\beta_0 = 1.12\%$ and $\beta = 0.535\%$. See table 2. Next, β values are obtained also for the discharges discussed in section 4.1. As a first example, for discharge #55313 (1 PI) of figure 4, $\beta_0 = 1.4\%$ and normalized $\beta = 0.68\%$ between 1182 ms and 1187 ms when TS and CXRS are performed and $W^E_{diag} = 3.4$ kJ, this being close to maximum for this discharge, *i.e.* 3.8 kJ. This discharge does not terminate until NBI switch-off; thus, slightly higher β values may have been attained later along this discharge. Nonetheless, it is apparent that a single PI results in significantly increased β's. As a second example, in discharge #55300 (2 PIs) and $W^E_{diag} = \sim 4.4$ kJ, see figure 6, which is representative of the highest diamagnetic energies achieved in TJ-II with counter-NBI heating only, $\beta_0 = 1.88\%$ and normalized $\beta = 0.94\%$. TS and CXRS measurements were performed just before the plasma begins a slow collapse, thus these β values are above but close to the maximum values that can be achieved in TJ-II with PIs and heating from a single NBI. The values can be compared also with empirically-based prediction

Table 2. Summary of plasma parameters for discharges described in sections 3.2 and 3.3. Discharge 55308 is a reference discharge from the same series as 55300 and 55313. Subscripts + and ++ in the first column represent 1 PI and 2 PIs, respectively. N_{e0}, T_{e0} and T_{i0} values are obtained using TS and CXRS, thus $n_{e0}/<n_e>$, β_0 and normalized β values are estimated when such measurements are made. $\tau_E{}^{diag}$ and $\tau_E{}^{ISS04}$ values are taken when $W^E{}_{diag}$ is maximum along each discharge.

Discharge	N_{e0} (10^{19} m^{-3})	T_{e0} (eV)	T_{i0} (eV)	$n_{e0}/<n_e>$	β_0 (%)	β_{norm} (%)	$W^E{}_{max}$ (kJ)	$\tau_E{}^{diag}$ (ms)	$\tau_E{}^{ISS04}$ (ms)	$\tau_E/\tau_E{}^{ISS04}$
55300^{++}	9.0	285	185	1.5	1.88	0.94	4.4	13.9	12.4	1.12
55308	3.2	300	130	1.41	0.6	0.32	2.0	9.0	9.8	0.92
55313^{+}	6.2	325	160	1.35	1.4	0.68	3.8	11.8	10.7	1.11
55511	5.8	325	115	1.32	1.12	0.535	3.0	8.5	10	0.85

limits, for instance, with the β limit predicted by Sudo's scaling, $\beta^{Sudo}(\%)$, where $\beta^{Sudo}(\%) = 0.55\ P_{abs}{}^{0.77}\ B^{-0.82}\ a^{-0.69}\ R^{-0.6} = \sim 0.56\%$ [51], which is in reasonable agreement with β measured for #55511 (no PI). However, significantly higher β values are achieved after PI(s), the maximum β achieved here being 0.94% for #55300. However, as noted, discharge #55300 collapses slowly after PI, thus Sudo β scaling predictions can be surpassed by a factor of up to 1.7 when PIs are performed into counter-NBI heated plasmas in TJ-II. In contrast, the normalized beta, stability/equilibrium β limit was predicted to be 3% for this 100_44_64 configuration with magnetic well = 2.27% [52]. Finally, technical issues with the co-counter NBI system have limited the PI experiments presented here to counter NBI heating discharges only. Thus, PIs into dual NBI-heated plasmas, which might produce even higher β values, still need to be studied and evaluated. It is intended to report such measurements once the technical issues with NBI#1 have been resolved.

4.3. Ion temperature

As presented in section 3.2, T_{e0} values in discharges #55300 (with PI) and #55511 (no PI) differ by about 15%, whereas central n_e and T_i values are ∼50% and ∼60% higher in discharge #55300. Similar tendencies are seen for discharge #55313 (with PI). In the case of discharges #55511 (no PI) and #55313 (with PI), TS and CXRS measurements are made at similar $<n_e>$, $\sim 4.4 \times 10^{19}$ m^{-3}. Indeed, T_{e0} and n_{e0} are quite similar for both of these discharges, whereas $T_{i0} = \sim 115$ eV for #55511 and $T_{i0} = \sim 165$ eV #55313. In order to understand this significantly higher T_{i0} in discharge #55313, it is necessary to consider several factors. First, it should be recalled that, the NBI beam has energy, E_{beam}, = 30 keV and a through-port full, half and third energy component ratio equal to 55:20:25. Also, for $E_{beam} = 30$ keV, fast-ion energy transfers principally to plasma electrons and is of the order 75% [53]. This percentage depends primarily on E_{beam} and T_e, whereas neutral-beam ion slowing-down depends on n_e and T_e. Thus, direct ion NBI-heating is expected to be quite similar for both of these situations. In contrast, the largest contribution to ion heating in TJ-II is electron-ion energy transfer, which is proportional to the difference between T_e and T_i and to the collisional transfer coefficient which is $\sim n_e{}^2\ T_e{}^{-3/2}$. Thus, comparing the T_e and T_i profiles for the discharges in figures 5 and 7, the observed reduction in the electron-ion temperature difference should reflect reduced ion heating, and hence lower ion radial heat fluxes during the PiEC phase. This, together with the larger ion energy content, should result in improved ion energy confinement.

4.4. Extended plasma performance after PIs

Experiments have been performed here using both single and multiple pellet injections, in some cases with the largest available cryogenic pellets. In section 3, it was reported that, compared to results published in [9]. (NBI heated plasmas without PI), significantly higher densities and stored diamagnetic energies, as well as longer confinement times, are reached in TJ-II after multiple pellet injections. Indeed, an upper density limit for sustaining high-performance plasma operation is approached here for the heating power available, thus it is interesting to compare current data with limits achieved without pellets and with empirical law predictions.

An extensive comparison of TJ-II NBI plasma data with empirical laws was presented in [19]. Therein, data were presented for co-, counter- and co- plus counter-NBI heating scenarios and for different wall coating conditions. However, as noted, comparisons are limited here to counter-NBI PI data with lithium wall coatings. For instance, in single PI experiments in [9], improvements up to 40% were achieved when $\tau_E{}^{diag}$ values were compared with $\tau_E{}^{ISS04}$ values. When current data and [9] data are considered, improvements in $\tau_E{}^{diag}$ up to ∼50% can be achieved after multi-pellet injections when compared with empirical law predictions, $\tau_E{}^{ISS04}$. See figure 12. This factor of ∼1.5 represent the current upper limit for injections into single beam NBI-heated plasmas.

It was reported in [9] that the bifurcation found in the plasma triple product, $n_e\ T_i\ \tau^E$, after a single pellet injection reached values that were significantly higher than those obtained by other plasma fuelling methods in TJ-II when experimental and ISS04 scaling branches were compared and that the higher branch was maintained until NBI switch-off. At that time, CXRS measurements were unavailable and it was assumed then that NPA measurements were representative of core T_i after PI. As noted in section 3.2, CXRS T_i values are significantly higher than recorded NPA T_i values after PI, as the latter are underestimated in the centre due to reduced fluxes of CX neutrals escaping from the post-injection high-density core region. However, only one T_i profile per discharge can be obtained on TJ-II with CXRS. Despite this limitation, plasma triple products with and without PIs can be compared now for a single time point. Here, plasma triple product values when

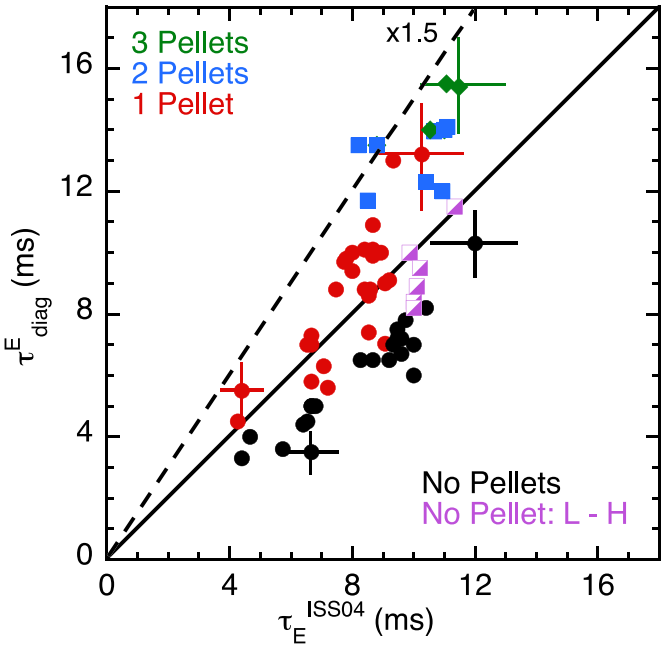

Figure 12. Diamagnetic energy confinement times for selected TJ-II discharges, $\tau_E{}^{diag}$, versus predicted ISS04 times, $\tau_E{}^{ISS04}$, estimated using equation (1). τ's are estimated when $W^E{}_{diag}$ is maximum along each discharge. Data are for counter NBI-heated plasmas with no PI (black dots), L-H type transition with no PI (lilac squares), and with 1 (red dots), 2 (blue squares) or 3 (green diamonds) PIs. The dash-dash line represents $\tau_E{}^{diag} = 1.5 \times \tau_E{}^{ISS04}$. Variations in injected pellet sizes and plasma conditions give rise to the spread in data for the same data types. Error bars are shown for selected data.

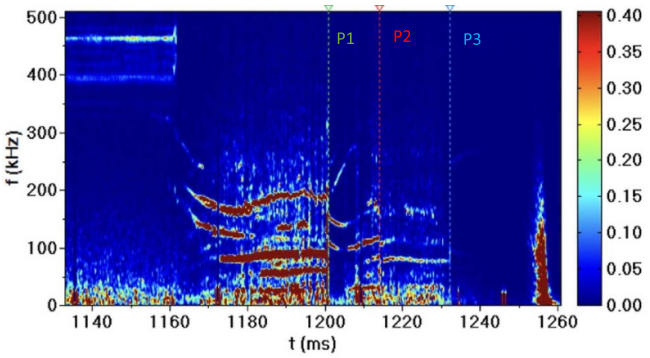

Figure 13. Fast-Fourier transform spectrogram of the secondary beam signal intensity measured by one HIBP system at $\rho = 0.5$ during TJ-II discharge #52582. Pellets containing 1.4×10^{19}, 5.5×10^{18} and 4×10^{18} H atoms are injected at 1200.4 ms (green dash-dash), 1213.9 ms (red dash-dash) and 1231.9 ms (light blue dash-dash), respectively.

CXRS is performed are 3.9×10^{-3} ($\times 10^{19}$ m^{-3} keV s) for #55511 (no PI), 5.6×10^{-3} ($\times 10^{19}$ m^{-3} keV s) for #55313 (1 large pellet), and 0.01 ($\times 10^{19}$ m^{-3} keV s) for #55300 (2 large pellets). The latter values represent a 43% increase if 1 large pellet is injected and a 170% increase if the 2 largest available pellets are injected when these values are compared with the triple product for #55511 at similar time instances. However, #55300 is not sustained until NBI switch-off so this may represent an upper limit. Nonetheless, the values are the highest triple product achieved to date in TJ-II.

Finally, in discharges with large PIs presented here, a density limit is reached after which the plasma decays. It is possible to compare this limit with data from [19] and with, for instance, Sudo's scaling law predictions, *i.e.* $<n_e>^{Sudo}$ [$\times 10^{20}$ m^{-3}] $= 0.25$ (P_{abs} B/a^2 R)$^{0.5}$ [51]. This law was based mainly on data from Heliotron E [54]. Since then, a number of other scaling relations have evolved as more data was collected [55, 56], nonetheless, the bulk of such data favour a (P B/V)$^{0.5}$ scaling. Thus, $<n_e>^{Sudo}$ is $\sim 5.8 \times 10^{19}$ m^{-3} for the NBI heated plasmas considered here. In the case of discharge #55511 (no PI) of figure 6, plasma quench commences when $<n_e>^{exp}$ is $\sim 5.2 \times 10^{19}$ m^{-3}, a factor of 0.9 lower than $<n_e>^{Sudo}$. In contrast, for #55300 (2 PIs), plasma decay begins when $<n_e>^{exp}$ is $\sim 6.2 \times 10^{19}$ m^{-3}, $\sim$1.2 times higher than for the reference discharge and $\sim$1.07 times higher than $<n_e>^{Sudo}$. Thus, the ratios $<n_e>^{exp}/n_e{}^{Sudo}$ and $\tau_E{}^{diag}/\tau_E{}^{ISS04}$ are both >1 for #55300 (2 PIs) whereas in [19], when $\tau_E{}^{diag}/\tau_E{}^{ISS04}$ was >1, $n_e{}^{exp}/n_e{}^{Sudo}$ was always $\leqslant 1$ as is found here for #55511. In both discharges, Z_{eff} is low, *i.e.* 1.1 for #55300 and 1.4 for #55511, thus the contribution of impurities to the plasma limit can be considered minor here. The findings reported in here confirm that diamagnetic energy confinement and plasma triple product can be further enhanced in TJ-II by the injection of additional pellets with time-gaps between injections similar to energy confinement times and indicate that PIs may also extend the TJ-II density limit beyond Sudo predictions. Experiments will be performed in the near future to elucidate more on density limits.

4.5. Reduction of plasma fluctuations

Finally, it was reported in [9] that PIs into NBI-heated plasmas result in clear transient reductions in density and potential fluctuations in the region around $\rho = 0.6$ where the strongest changes in plasma density gradient were observed. Here, in figure 3, when reference discharge #52580 and pellet discharges #52588 and #52586 are compared, the latter discharges display more negative density gradients about the same radial region. In a discharge of the same experiment, #52582, density turbulence measured at $\rho = 0.5$ by HIBP#1 is suppressed by an initial large pellet (P1), then recovers partially, before finally being reduced further by the second (P2) and supressed third pellets (P3). See figure 13. Similarly, measurements made for discharge #55300 using the Doppler Reflectometer also show suppressed fluctuations at $\rho = 0.85$ after PIs. See figure 14. Although the contribution of turbulence to improved performance still remains to be quantified (efforts are being made currently for a future publication), NC calculations made for discharges #55511(no PI) and #55300 (2 large PIs) using the kinetic profiles of figure 7 and the Z_{eff} reported in section 3.2 [57–59], show that the NC energy confinement time, $\tau^E{}_{neo}$, approaches $\tau_E{}^{diag}$ for #55300 ($\tau_E{}^{diag} = 14.5$ ms and $\tau_E{}^{neo} = 18$ ms), whereas there exists a large discrepancy between them for #55511 ($\tau_E{}^{diag} = 8.2$ ms

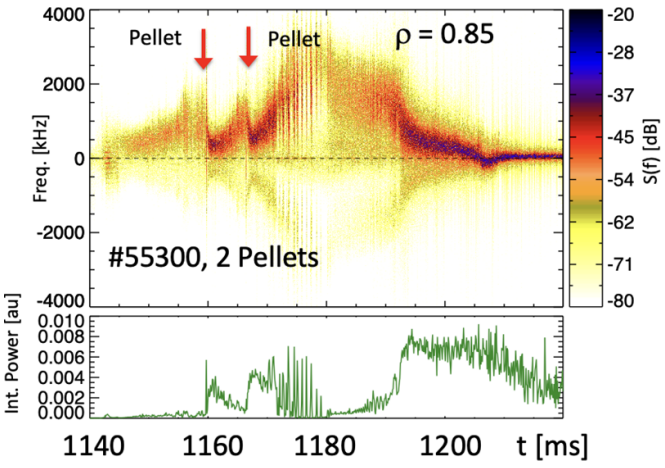

Figure 14. Spectrogram of the Doppler Reflectometer signal at $\rho = \sim 0.85$ for discharge #55300 and plot of total scattered power. Pellets containing 2×10^{19} and 1.8×10^{19} H atoms are injected at 1159.8 ms and 1166 ms, respectively.

and $\tau_E{}^{neo} = 22$ ms). Indeed, since plasma potential and density turbulence are reduced strongly after multiple pellet injections, the closer agreement between $\tau_E{}^{diag}$ and $\tau_E{}^{neo}$ might indicate that plasma #55300 is approaching NC conditions whereas #55511 is still turbulence dominated. Similar conclusions were drawn after PIs into W7-X where it was considered that post-injection high performance plasmas approached NC conditions [13]. However, it is considered that TJ-II plasmas are far from ITG instabilities, thus the identification underlying phenomena in TJ-II requires further work. Further investigation of this in underway and will be reported in the future.

5. Summary

In this paper, the PiEC performance phase reported previously for single pellet injection into NBI heated TJ-II plasmas has been extended by performing multiple pellet injections. It is found that the injection of additional small pellets into TJ-II allows PiEC phases with plasma densities higher than those reached previously with a single pellet to be achieved and maintained until NBI switch-off. In addition, it has been demonstrated, for instance, that pellet-induced improved performance in TJ-II is independent of NBI heating direction, *i.e.* of counter or co-counter injection. Moreover, through the availability of a CXRS diagnostic, it has been found that core ion temperature values increase significantly after pellet injection(s) when compared with NBI-heated reference discharges with similar line-averaged density It is considered that a reduction in the electron-ion temperature difference results in lower ion heating and hence lower ion radial heat fluxes. This, together with a larger ion energy content, results in improved ion energy confinement. In addition, results show that diamagnetic energy confinement times are further enhanced by the injection of additional pellets with time-gaps between injections similar to energy confinement times while also indicating that PIs can push the experimental density limit beyond Sudo predictions. Finally, record values for $W^E{}_{diag}$ and n_{e0}, as well as for central and normalized β, have been attained here for TJ-II plasmas after multiple pellet injections. These values may be limited here by the availability of only a single NBI system (due to technical issues). Thus, it is intended to repeat these studies when both NBI systems are available. Finally, whilst some basic arguments are presented here to explain the observed tendencies, local power balance analysis as well as gyrokinetic and MHD resistive modelling will be the subject of future studies to quantify and understand better ion heat diffusivity and main instabilities that may be playing a role in these phenomena.

Acknowledgments

This work has been carried out within the framework of the EUROfusion Consortium, funded by the European Union via the Euratom Research and Training Programme (Grant Agreement No. 101052200—EUROfusion). Views and opinions expressed are however those of the author(s) only and do not necessarily reflect those of the European Union or the European Commission. Neither the European Union nor the European Commission can be held responsible for them. This work is partially financed by grant PID2020-116599RB-I00 funded by MCIN/AEI/10.13039/501100011033 and by ERDF A way of Making Europe. O.O. Chmyga and O.S. Kozachok strongly appreciate financial support from CIEMAT during their stay at LNF-CIEMAT during 2022 and 2023. The authors acknowledge contributions to HIBP data collection, analysis and interpretation made by A. Melnikov, M. Drabinskiy, L.G. Eliseev and P. Khabanov as part of the long-term trilateral collaboration between National Research Center 'Kurchatov Institute,' Moscow, Russia, led by S. Melnikov, the HIBP group from Kharkov Institute of Physics and Technology, Kharkov, Ukraine, led by L.I. Krupnik and CIEMAT.

ORCID iDs

K.J. McCarthy https://orcid.org/0000-0002-5881-1442
I. García-Cortés https://orcid.org/0000-0002-5223-391X
J.A. Alonso https://orcid.org/0000-0001-6863-8578
A. Baciero https://orcid.org/0000-0003-1717-3509
A. Cappa https://orcid.org/0000-0002-2250-9209
T. Estrada https://orcid.org/0000-0001-6205-2656
R. García https://orcid.org/0009-0009-6063-5255
B. López Miranda https://orcid.org/0000-0003-4236-7727
B. van Milligen https://orcid.org/0000-0001-5344-6274
M.A. Ochando https://orcid.org/0000-0001-7521-4503
I. Pastor https://orcid.org/0000-0003-0891-0941

References

[1] Baylor L.R., Parks P.B., Jernigan T.C., Caughman J.B., Combs S.K., Foust C.R., Houlberg W.A., Maruyama S. and Rasmussen D.A. 2007 *Nucl. Fusion* **47** 443
[2] Combs S.K. and Baylor L.R. 2018 *Fusion Sci. Technol.* **73** 493
[3] Pégourié B. 2007 *Plasma Phys. Control. Fusion* **49** R87
[4] Lang P.T. *et al* 2018 *Nucl. Fusion* **58** 036001
[5] Belokurov A.A. *et al* 2018 *Nucl. Fusion* **58** 112007

[6] Beidler C.D. *et al* 2021 *Nature* **596** 221
[7] Bozhenkov S.A. *et al* 2020 *Nucl. Fusion* **60** 066011
[8] Hidalgo C. *et al* 2022 *Nucl. Fusion* **62** 042025
[9] García-Cortés I. *et al* 2023 *Phys. Plasmas* **30** 072506
[10] Sakamoto R. *et al* 2001 *Nucl. Fusion* **41** 381
[11] Baldzuhn J. *et al* 2020 *Plasma Phys. Control. Fusion* **62** 055012
[12] Pedersen T.S. *et al* 2019 *Plasma Phys. Control. Fusion* **61** 014035
[13] Estrada T. *et al* 2021 *Nucl. Fusion* **61** 046008
[14] Kaneko O. *et al* 2009 *Plasma Fusion Res.* **4** 27
[15] McCarthy K.J. *et al* 2017 *Europhys. Lett.* **120** 25001
[16] Panadero N. *et al* 2018 *Nucl. Fusion* **58** 026025
[17] McCarthy K.J. *et al* 2017 *Nucl. Fusion* **57** 056039
[18] Yamada H. *et al* 2005 *Nucl. Fusion* **45** 1684
[19] Ochando M.A. *et al* 2014 *Proc. 41st EPS Conf. on Plasma Physics* (European Physical Society) p P2.074
[20] García L., García-Cortés I., Carreras B.A., McCarthy K.J. and van Milligen B.P. (TJ-II Team) 2023 *Phys. Plasmas* **30** 092303
[21] Hutchinson I.H. 1987 *Principles of Plasma Diagnostics* (Cambridge University Press)
[22] Matsuyama A., Koechl F., Pégourié B., Sakamoto R., Motojima G. and Yamada H. 2012 *Plasma Fusion Res. Lett.* **7** 1303006
[23] Liniers M. *et al* 2013 *Fusion Eng. Des.* **88** 960
[24] Tabarés F.L. *et al* 2010 *Contrib. Plasma Phys.* **50** 610
[25] Combs S.K. *et al* 2013 *Fusion Sci. Technol.* **64** 513
[26] McCarthy K.J. 2021 *J. Instrum.* **16** C12026
[27] Herranz J., Castejón F., Pastor I. and McCarthy K.J. 2003 *Fusion Eng. Des.* **65** 525
[28] Jiménez-Gómez R. *et al* 2011 *Nucl. Fusion* **51** 033001
[29] Baião D., Medina F., Ochando M., McCarthy K., Tabarés F., Pastor I. and Varandas C. 2012 *Rev. Sci. Instrum.* **83** 053501
[30] Happel T., Estrada T., Blanco E., Tribaldos V., Cappa A. and Bustos A. 2009 *Rev. Sci. Instrum.* **80** 073502
[31] Melnikov A.V. *et al* 2015 *Fusion Eng. Des.* **96–97** 724
[32] Melnikov A.V. *et al* 2017 *Nucl. Fusion* **57** 072004
[33] Melnikov A.V. *et al* 2013 *Nucl. Fusion* **53** 092002
[34] Carmona J.M., McCarthy K.J., Balbín R. and Petrov S. 2006 *Rev. Sci. Instrum.* **77** 10F107
[35] McCarthy K.J., Panadero N., López-Fraguas A., Hernández J. and van Milligen B. 2015 *Contrib. Plasma Phys.* **55** 459
[36] McCarthy K.J., Zurro B., Balbín R., Baciero A., Herranz J. and Pastor I. 2003 *Europhys. Lett.* **63** 49
[37] Zurro B., Baciero A., Liniers M. and Cappa A. (TJ-II Team) 2010 *Contrib. Plasma Phys.* **50** 616
[38] Arévalo J., Alonso J.A., McCarthy K.J. and Velasco J.L. 2013 *Nucl. Fusion* **53** 023003
[39] Van Milligen B.P., Nicolau J.H., García L., Carreras B.A. and Hidalgo C. the TJ-II Team 2017 *Nucl. Fusion* **57** 056028
[40] McCarthy K.J. *et al* 2021 *Nucl. Fusion* **61** 076014
[41] Panadero N., McCarthy K.J., Pégourié B., Carrasco R., García-Cortés I., García R., Hernández-Sánchez J., Köchl F., Mártinez-Fernández J. and Sakamoto R. 2023 *J. Plasma Phys.* **89** 955890601
[42] García-Cortés I. *et al* 2000 *Nucl. Fusion* **40** 1867
[43] Estrada T. *et al* 2009 *Plasma Phys. Control. Fusion* **51** 124015
[44] Ascasíbar E. *et al* 2010 *Contrib. Plasma Phys.* **50** 594
[45] Guasp J. and Liniers M. 1995 Comportamiento de las peŕdidas instantáneas y retardadas en la inyeccioń de neutros del TJ-II *Informes Técnicos Ciemat 761, Ciemat. Madrid* (in Spanish)
[46] Guasp J., Liniers M., Fuentes C. and Barrera G. 1999 *Fusion Sci. Technol.* **35** 32
[47] Guasp J., Fuentes C. and Liniers M. 2004 Cálculos de inyección de haces neutros para las descargas de TJ-II *Informes Técnicos Ciemat 1050, Ciemat. Madrid* (in Spanish)
[48] Vertkov A.V., Lyublinski I.E., Tabarés F. and Ascasíbar E. 2012 *Fusion Eng. Des.* **87** 1755
[49] Medina F., Ochando M.A., Baciero A. and Guasp J. 2007 *Plasma Phys. Control. Fusion* **49** 385
[50] Ascasíbar E., Estrada T., Castejón F., López-Fraguas A., Pastor I., Sánchez J., Stroth U. and Qin J. (TJ-II Team) 2005 *Nucl. Fusion* **45** 276
[51] Sudo S., Takeiri Y., Zushi H., Sano F., Itoh K., Kondo K. and Iiyoshi A. 1990 *Nucl. Fusion* **30** 11
[52] Varias A., Alejaldre C., Fraguas A.L., García L., Carreras B.A., Dominguez N. and Lynch V.E. 1990 *Nucl. Fusion* **30** 2597
[53] Speth E. 1989 *Rep. Prog. Phys.* **52** 57
[54] Sudo S. *et al* 1985 *Nucl. Fusion* **25** 94
[55] Wagner F. 1997 *Plasma Phys. Control. Fusion* **39** A23
[56] Giannone L. *et al* 2000 *Plasma Phys. Control. Fusion* **42** 603
[57] Tribaldos V. 2001 *Phys. Plasmas* **8** 1229
[58] Tribaldos V., Beidler C.D., Turkin Y. and Maassberg H. 2011 *Phys. Plasmas* **18** 102507
[59] Turkin Y., Beidler C.D., Maassberg H., Murakami S., Tribaldos V. and Wakasa A. 2011 *Phys. Plasmas* **18** 022505